

Generative AI Enabled Robust Sensor Placement in Cyber-Physical Power Systems: A Graph Diffusion Approach

Changyuan Zhao, Guangyuan Liu, Bin Xiang, Dusit Niyato, *Fellow, IEEE*, Benoit Delinchant, Hongyang Du, Dong In Kim, *Fellow, IEEE*

Abstract—With advancements in physical power systems and network technologies, integrated Cyber-Physical Power Systems (CPPS) have significantly enhanced system monitoring and control efficiency and reliability. This integration, however, introduces complex challenges in designing coherent CPPS, particularly as few studies concurrently address the deployment of physical layers and communication connections in the cyber layer. This paper addresses these challenges by proposing a framework for robust sensor placement to optimize anomaly detection in the physical layer and enhance communication resilience in the cyber layer. We model the CPPS as an interdependent network via a graph, allowing for simultaneous consideration of both layers. Then, we adopt the Log-normal Shadowing Path Loss (LNSPL) model to ensure reliable data transmission. Additionally, we leverage the Fiedler value to measure graph resilience against line failures and three anomaly detectors to fortify system safety. However, the optimization problem is NP-hard. Therefore, we introduce the Experience Feedback Graph Diffusion (EFGD) algorithm, which utilizes a diffusion process to generate optimal sensor placement strategies. This algorithm incorporates cross-entropy gradient and experience feedback mechanisms to expedite convergence and generate higher reward strategies. Extensive simulations demonstrate that the EFGD algorithm enhances model convergence by 18.9% over existing graph diffusion methods and improves average reward by 22.90% compared to Denoising Diffusion Policy Optimization (DDPO) and 19.57% compared to Graph Diffusion Policy Optimization (GDPO), thereby significantly bolstering the robustness and reliability of CPPS operations.

Index Terms—Generative AI, cyber-physical power system, sensor placement, diffusion model.

I. INTRODUCTION

In previous years, advances in control theory and infrastructure improvements within power grids have significantly improved the efficiency and reliability of monitoring and controlling the physical power system [1]. Simultaneously,

computer science and electronics techniques are enhancing cyber systems to improve the performance of computing and communication technologies. These parallel advances in both the physical power system and cyber systems are merging to form an integrated Cyber-Physical Power System (CPPS), which promises to revolutionize the management and operation of modern power grids [2]. CPPS is a novel system that integrates the internet and physical power system components, encompassing all aspects of electric power systems, including generation, transmission, distribution, and utilization [3], [4]. Nowadays, CPPS has been widely applied to various safety-critical power grid scenarios. Especially in power grid safety control, CPPS has a faster processing capability to ensure the overall safe operation of the power grid through cyber network analysis. Correspondingly, this also presents additional requirements from both physical and cyber perspectives for deploying components in the CPPS [5].

Anomaly detection is essential to prevent potential system failures and ensure the safety of CPPS. Recent progress in academia has significantly advanced the development of CPPS for anomaly detection. Li et al. [6] proposed an online anomaly detection method to accurately detect when an electrical component has failed based on a graph structure algorithm. With the rise of Artificial Intelligence (AI) technology, the CPPS anomaly detection framework has extensively incorporated machine learning and deep learning methods. For instance, Niu et al. [7] combined a long short term memory network and a convolutional neural network to develop a time-series anomaly detector for data injection attack detection. For these anomaly detection methods, efficient acquisition of real-time grid data requires advanced deployment of physical hardware. Hooi et al. [8] proposed an approach for sensor placement to maximize the probability of detecting anomalies with limited equipment.

In addition to deploying hardware, it is critical for the cyber layer to maintain communication between edge devices during disruptions caused by various destruction, including physical failures, natural disasters, and malicious attacks, ensuring the proper functioning of the system. The cyber layer's robustness typically depends on the topology structure of the network, which can be assessed using various metrics. For instance, Schneider et al. [9] proposed a robustness metric based on the percolation theory, which considers the maximal connected subgraphs after the repeated removal of the highest degree node. According to this robustness, Qiu et al. presented the

C. Zhao is with the College of Computing and Data Science, Nanyang Technological University, Singapore, and CNRS@CREATE, 1 Create Way, 08-01 Create Tower, Singapore 138602 (e-mail: zhao0441@e.ntu.edu.sg).

G. Liu and D. Niyato are with the College of Computing and Data Science, Nanyang Technological University, Singapore (e-mail: liug0022@e.ntu.edu.sg; dniyato@ntu.edu.sg).

B. Xiang and B. Delinchant are with CNRS@CREATE, 1 Create Way, 08-01 Create Tower, Singapore, 138602 (e-mail: bin.xiang@cnrsatcreate.sg; zabenoit.delinchant@grenoble-inp.fr)

H. Du is with the Department of Electrical and Electronic Engineering, University of Hong Kong, Hong Kong, China (e-mails: duhy@eee.hku.hk).

D. I. Kim is with the Department of Electrical and Computer Engineering, Sungkyunkwan University, Suwon 16419, South Korea (email:dikim@skku.ac.kr).

ROSE, a robustness strategy for scale-free wireless sensor networks [10]. Moreover, Zhang et al. proposed the r-robustness of the networks guaranteeing connectivity even if some nodes are removed [11].

Despite the significant progress, few papers investigate physical layer deployment and cyber layer communication connection simultaneously, i.e., *co-design a secure sensor placement strategy for anomaly detection and a robust communication protocol*. There are two difficult challenges that need to be addressed to resolve this problem

- **Challenge 1:** Anomaly detection in CPPS needs to prioritize accuracy with limited resources [3]. First, a limited number of sensors should be placed at the most critical nodes to ensure effective data extraction. Moreover, dispersing sensors will significantly increase the monitoring of every part of the power grid, but the connectivity and robustness of the network will be limited due to long wireless communication links. On the other hand, concentrating sensors will ensure the network’s connectivity but affect the detection accuracy [12]. Consequently, an effective sensor placement must consider both the physical and cyber layers to find a trade-off.
- **Challenge 2:** Sensor placement and robust network connection problems are typically challenging to solve. It has been proven that many optimizations that both optimize the node selection and the robustness of networks are non-deterministic polynomial-time hardness (NP-hard) [11]. Hence, many current solution algorithms are based on greedy algorithms or traditional optimization methods, which do not guarantee the optimal placement strategy [13]. Therefore, data-driven approaches, e.g., machine learning methods, become a preferred solution over mathematical model-based approaches to explore the global optimal solution.

In this paper, we present an efficient framework for placing sensors for anomaly detection and guaranteeing robustness under link failures in CPPS. First, we consider a one-to-one interdependent CPPS, where each node in the physical layer is controlled by one cyber node [14]. Next, we examine the edge robustness of the cyber layer, which refers to the ability to remain connected even when some edges are failed and disconnected. To measure it, we introduce two metrics: the Cheeger constant and the Fiedler value [15]. These metrics are mathematical indicators in graph theory that measure the edge connectivity of a graph, which in turn helps assess the robustness of the cyber layer. For the physical layer, we utilize power detectors for anomaly detection introduced in Grid-Watch [8]. Based on considerations at both the cyber layer and the physical layer, we formulate the robust sensor placement problem as an optimization to maximize the robustness of the cyber layer while ensuring accurate and effective anomaly detection in the physical layer. We utilize the Reinforcement Learning (RL) framework to efficiently find near-optimal solutions, which is suitable for the solution space is vast and not easily navigable through traditional optimization techniques [16]. Additionally, diffusion-based policy RL algorithms have

demonstrated state-of-the-art performance, particularly in network optimization contexts [17]. The diffusion model employs a unique combination of diffusion and denoising processes to effectively explore the search space to navigate through potential solutions, progressively refining decisions through the denoising phase to converge on optimal strategies. To solve the long time for the diffusion model convergence, we proposed an Experience Feedback Graph Diffusion (EFGD) policy optimization approach to solve the proposed secure sensor placement optimization. The proposed framework utilizes reinforcement learning from human feedback (RLHF) to improve the convergence speed of training by leveraging prior exploration feedback, which informs the optimization strategy in moving closer to the optimal outcome [18]. Our main contributions are summarized as follows.

- By using graph theory, we model a one-to-one interdependent CPPS [19] through the grid graph and communication graph with shared vertices, representing the potential location to place sensors. We introduce the Cheeger constant and the Fiedler value to measure the robustness of the cyber layer communications under link failures. Moreover, we utilize anomaly detectors in the physical layer to detect the abnormal power information of the power grid. *To the best of our knowledge, this is the first work that considers both the physical layer grid and the cyber layer network robustness simultaneously in CPPS for anomaly detection.*
- Based on the CPPS model, we formulate an optimization to maximize the robustness of the cyber layer network while ensuring accurate and effective anomaly detection in the power grid. We prove that the formulated problem is NP-hard, making it difficult to solve using existing optimization methods. Inspired by the diffusion model-based optimization framework [17], we design an optimization framework utilizing graph diffusion to optimize the placement policy via the denoising process.
- Due to the long time for the diffusion model convergence, we propose the EFGD policy optimization algorithm, which adopts the cross-entropy gradient and introduces experience feedback into the training. Instead of using the negative log-likelihood gradient, the proposed EFGD approach utilizes the cross-entropy gradient, allowing it to explore higher rewards and bring the predicted distribution closer to the latent distribution. Moreover, the inclusion of experiment feedback in the EFGD method can significantly improve the convergence during training.

The rest of the paper is organized as follows. Section II reviews related works. The CPPS system model consisting of both physical layer and cyber layer is presented in Section III. In Section IV, we first formulate the robust sensor placement optimization problem for anomaly detection. Then, we elaborate on the design of EFGD to solve the optimization problem effectively. Section V provides and discusses the simulation results. Finally, Section VI summarizes the paper.

II. BACKGROUND AND RELATED WORK

Interdependent CPPS frameworks are crucial for modernizing and enhancing power infrastructure robustness through

the integration of computational and physical processes. A common application is the one-to-one interdependent CPPS, where each physical layer node in the physical layer is controlled by a cyber node [14]. The physical layer of the CPPS comprises power consumption and/or production nodes connected with lines. Some selected nodes in the physical layer function as a sensor that collects and monitors the status information, such as current and voltage. Through one-to-one interdependency, each sensor transmits the collected information to the corresponding information transmission unit. Subsequently, the transmission unit of each node sends the information to the unified power grid control center via the cyber layer’s communication link. Finally, the power grid control center processes and analyzes the collected data and controls the CPPS based on the analysis results.

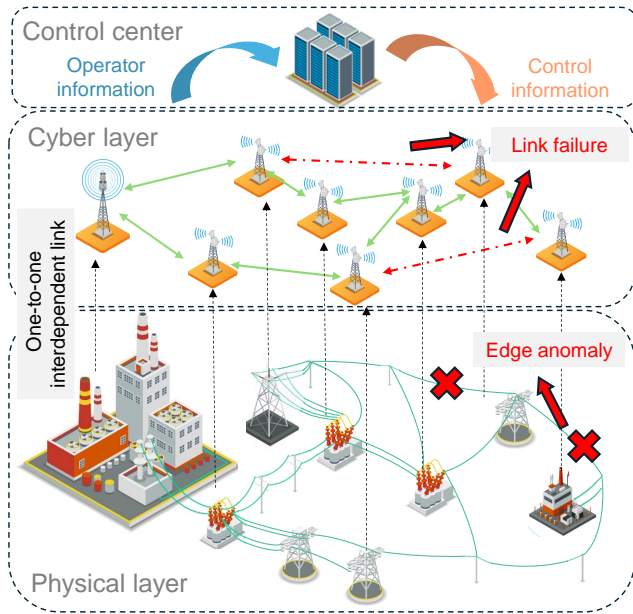


Fig. 1: The system model of interdependent CPPS. Part A. The illustration of the physical layer grid with edge anomaly. Part B. The cyber layer network with link failures. Part C. The control center processes data and controls the CPPS.

A. Anomaly Detection in Physical Layer

Anomaly detection for the physical layer of CPPS aims to identify changes in the physical information of the circuit, such as voltage and current, to achieve grid monitoring. Time series anomaly detection is a common method used in practice focusing on the temporal characteristics of circuit information [20]. For multivariate time series, there are numerous techniques to achieve detection, including convolutional neural networks [21], autoencoder models [22], distance-based models [23], and isolation forests [24]. Additionally, temporal graph anomaly detection utilizes the topology structure to find anomalous changes in the grid, such as neighborhood-based [25] and community-based approaches [26]. For dynamic graphs [6], the authors in [27] found change points, while other researchers leveraged partition-based [28] and sketch-based [29] approaches. However, almost all these methods require

fully observed data from deployed sensors and only seldom consider sensor selection or placement for effective detection [8]. Moreover, the papers on sensor placement only consider one aspect of the grid system, such as state estimation [30], without considering the transmission simultaneously. Motivated by this situation, we intend to provide a sensor placement approach for effective anomaly detection and enhance the transmission robustness simultaneously.

B. Robust Network in Cyber Layer

The primary function of the CPPS cyber layer is to transmit, calculate, and collect data. Therefore, robust networks prioritize maintaining the specific operation of the entire network, even in the face of disruptions such as link failures or node damage. Researchers usually use graphs to illustrate the topological structure of networks, utilizing various graph properties to verify and enhance network robustness [31]. Based on the percolation theory, the authors in [9] proposed a robustness metric to measure network robustness under node failures. Additionally, by utilizing this robustness metric, a robust generation strategy for wireless communication networks is proposed, which significantly enhances the robustness of the network against nodes cyberattacks [10], [32]. Besides node failures, the authors in [33] measured the availability of planned networks by analyzing the number of redundant nodes. This method enhances network reliability for any given topology by increasing redundant nodes. However, it cannot ensure that the total number of nodes remains below a specific level. Therefore, we utilize metrics, including the Cheeger constant and the Fiedler value in graph theory, to assess the robustness of a graph with link failures. These metrics are related to the structure of the graph rather than the number of nodes, allowing for a better trade-off between the number of nodes and the overall network structure [15].

C. Diffusion Model-based Network Optimization

Diffusion models are generative AI models that have recently gained significant attention. They can learn data distribution by gradually introducing noises and removing them through a denoising process [34]. Due to their remarkable feature learning ability, diffusion models have been widely used in various tasks, such as image generation, video generation, and audio generation [35]. Recently, researchers have started extending the diffusion model to tasks beyond generation, such as integrating denoising process with the RL framework [36]. Du et al. [17] proposed a diffusion model-based RL framework for network optimization whose scalability and excellent performance have surpassed many existing RL methods in wireless communication tasks [37]. Due to the topological nature of communication networks, network optimization problems are usually represented using graph structures. Liu et al. [38] proposed a Graph Diffusion Policy Optimization (GDPO) method to optimize the generated graph. GDPO can also effectively address problems under given constraints in wireless networks [39]. However, limited by the slow convergence of the diffusion model, these methods usually require a long training time [40]. In this paper, we

present a novel policy function combined with experiment feedback, which guides each step to the optimal generated graph, leading to better convergence results.

III. SYSTEM MODEL: INTERDEPENDENT CYBER-PHYSICAL POWER SYSTEMS FOR ANOMALY DETECTION

In this section, we present our interdependent CPPS model designed for accurate anomaly detection and robust data transmission.

A. Interdependent Cyber-Physical Power System Model

The proposed CPPS consists of a physical layer, which is a transmission grid, and a cyber layer modeled by a wireless sensor network (WSN). As shown in Fig. 1, we consider a one-to-one interdependent CPPS model [14]. The physical layer is formally represented by a graph $\mathcal{G}_P = (\mathcal{V}_P, \mathcal{E}_P)$, where \mathcal{V}_P denotes the set of grid nodes in which the sensors can be placed, and \mathcal{E}_P is the set of nodes connectors (electrical lines), as shown in Fig. 1 *Part A*. Similarly, we model the WSN cyber layer by another graph $\mathcal{G}_C = (\mathcal{V}_C, \mathcal{E}_C)$, where \mathcal{V}_C represents the set of potential locations for data transmission units, and \mathcal{E}_C denotes the set of corresponding communication links (Fig. 1 *Part B*). To achieve effective one-to-one interdependent transmission, we assume the grid sensor in the physical layer and its corresponding data transmission unit in the cyber layer are placed on the same node. Thus, the choice of nodes where sensors may be deployed should also be the same, i.e., $\mathcal{V}_P = \mathcal{V}_C$. For convenience, we use \mathcal{V} jointly to represent this set of vertices where sensors can be placed. Moreover, we consider one power grid control center in the CPPS, which monitors the operation of the CPPS and sends control instructions through the connection with the cyber layer. (Fig. 1 *Part C*).

B. Cyber Layer Model for Robust Communication

In this subsection, we will present our cyber layer model for robust communication.

1) *Communication Link*: We first consider reliable communication links between access nodes within the cyber layer, which can be measured by various metrics. In this paper, we utilize the Log-Normal Shadowing Path Loss (LNSPL) model to assess the communication quality of links, which can be generalized to various environments, including indoor, inter-vehicular, and near-ground scenarios [41].

In the cyber layer $\mathcal{G}_C = (\mathcal{V}, \mathcal{E}_C)$, we use a matrix $D = \{d_{i,j}\}$ to denote the distance between each node, where $d_{i,j}$ represents the physical distance between nodes v_i and v_j in the set of vertices \mathcal{V} . Accordingly, the path loss PL of the communication link between v_i and v_j can be expressed as [42]

$$PL(v_i, v_j) = BPL(d_0) + 10 \cdot \gamma \cdot \log_{10}\left(\frac{d_{i,j}}{d_0}\right) + X_\sigma, \quad (1)$$

where $BPL(d_0)$ represents the reference path loss of distance d_0 , γ is the path loss exponent reflecting the rate at which the signal attenuates with distance, and X_σ is a zero mean

Gaussian random variable with the variance of σ , denoting the shadow fading. In this model, the signal-to-noise ratio $SNR(v_i, v_j)$ from the transmitter v_i is given by

$$SNR(v_i, v_j) = P_t(v_i) - PL(v_i, v_j) - P_n, \quad (2)$$

where P_t and P_n represent the transmit power and noise power. Since we are in the placement stage, we assume that the transmission power of each sensor consistently reaches the minimum P_t^m and the noise power remains uniform across all communication links at the worst case P_n^M . Consequently, the SNR we calculated is based on the worst transmission conditions, serving as a lower bound to ensure safe operation after placement. Under this assumption, to maintain reliable communication links, the communication link is active between two nodes only if the value of the signal-to-noise ratio is high, i.e., the path loss does not exceed a certain threshold. Given a threshold λ_c , the communication state $l_{i,j}$ between nodes v_i and v_j can be written as

$$l_{i,j} = \begin{cases} 1, & PL(v_i, v_j) \leq \lambda_c \wedge (v_i, v_j) \in \mathcal{E}_C, \\ 0, & \text{otherwise,} \end{cases} \quad (3)$$

where $l_{i,j} = 1$ indicates the activated link, $l_{i,j} = 0$ represents the link is not activated, and $(v_i, v_j) \in \mathcal{E}_C$ indicates the link is in the set of potential communication links, as demonstrated in Fig. 2 *Part B*.

2) *Robust Network*: In this part, we present several critical metrics for evaluating the robustness of communication networks. We consider the robustness of the cyber layer to ensure that network communication remains reliable and functional. Specifically, we measure the robustness of the network as a capability to maintain connectivity even when some of its links fail [43]. In this paper, we leverage the Cheeger constant of the graph as the performance indicator. The Cheeger constant, also known as the Isoperimetric number, measures the weak connections in a graph, where a higher Cheeger constant indicates better connectivity and fewer bottlenecks [44].

Considering the cyber layer graph $\mathcal{G}_C = (\mathcal{V}, \mathcal{E}_C)$, $E_C = \{\alpha_{i,j}\}_{n \times n}$ is a 0-1 adjacency matrix of \mathcal{G}_C , where n represents the number of vertices, i.e., $n = |\mathcal{V}|$, and $\alpha_{i,j}$ equals 1 if vertices v_i and v_j are connected, and 0 otherwise. $D = \text{diag}\{\beta_1, \dots, \beta_n\}$ is the degree matrix of the cyber layer, where $\beta_i = \sum_{1 \leq j \leq n, j \neq i} \alpha_{i,j}$ represents the degree of vertex $v_i \in \mathcal{V}$. Given the adjacency matrix E_C and the degree matrix D , the Laplacian matrix of graph \mathcal{G}_C can be expressed as $L_{\mathcal{G}_C} = D - E_C$. For the normalized Laplacian matrix $\mathcal{L}_{\mathcal{G}_C} = D^{-1/2} L_{\mathcal{G}_C} D^{-1/2}$, the Cheeger constant in spectral graph theory is defined as [45]:

$$h(\mathcal{L}_C) = \min_{\mathcal{Y}} \frac{\sum_{i \in \mathcal{Y}, j \in \bar{\mathcal{Y}}} \alpha_{i,j}}{\min\{\text{vol}(\mathcal{Y}), \text{vol}(\bar{\mathcal{Y}})\}}, \quad (4)$$

where $h(\mathcal{L}_{\mathcal{G}_C})$ indicates the Cheeger constant of graph \mathcal{L}_C , $\mathcal{Y} \subset \mathcal{V}$ is a subset of the nodes and $\text{vol}(\mathcal{Y}) = \sum_{i \in \mathcal{Y}} \beta_i$ denotes the volume of node set \mathcal{Y} . However, the computation of the Cheeger constant for a given graph is NP-hard, leading to a substantial computational complexity in the subsequent sensor placement [46].

Therefore, we utilize the bounds of the Cheeger constant

to provide an approximate guarantee, which can be computed by the Cheeger's inequality. The Cheeger's inequality can be written as [15]:

$$\lambda_2(\mathcal{L}_{\mathcal{G}_C})/2 \leq h(\mathcal{L}_{\mathcal{G}_C}) \leq \sqrt{2\lambda_2(\mathcal{L}_{\mathcal{G}_C})}, \quad (5)$$

where $\lambda_2(\mathcal{L}_C)$ denotes the second smallest eigenvalue of the network Laplacian matrix \mathcal{L}_C . Let $\mathbf{0}$ and $\mathbf{1}$ represent the vectors with all coordinates equal to 0 and 1, respectively, the eigenvalue can be computed by [15]:

$$\lambda_2(\mathcal{L}_{\mathcal{G}_C}) = \min_{v \neq \mathbf{0}, v \perp \mathbf{1}} \frac{\langle \mathcal{L}_{\mathcal{G}_C} v, v \rangle}{\langle v, v \rangle}. \quad (6)$$

Additionally, the second smallest eigenvalue of $\lambda_2(\mathcal{L}_{\mathcal{G}_C})$ is referred to as the Fiedler value of the graph, which has a specific connection to the connectivity of the graph [15], as shown in Fig. 2 Part C.

C. Physical Layer Model for Anomaly Detection

In this subsection, we will introduce our detailed physical layer model designed for anomaly detection.

1) *Sensor Information Collection*: When an anomaly occurs in the physical layer of CPPS, such as a transmission line failing or a grid component failing, the voltages at some nodes and the currents along the edges of the grid will change [47]. By placing sensors on the grid nodes, the voltage and current changes of the grid can be measured.

To be more specific, consider the physical layer graph $\mathcal{G}_P = (\mathcal{V}, \mathcal{E}_P)$. For a grid sensor deployed at vertex $v_i \in \mathcal{V}$, it can measure the voltage $V_i(t) \in \mathbb{C}$ of node v_i at time t . Furthermore, it can also measure the current $I_e(t) \in \mathbb{C}$ along the edge $e \in \mathcal{N}_i$, where $\mathcal{N}_i \subseteq \mathcal{E}_P$ denotes the set of edges adjacent to the vertex v_i . Compared with directly analyzing the changes in current and voltage, the power of the node combines the characteristics of both information. Therefore, the state of power can simultaneously indicate the changing characteristics of current and voltage, providing better anomaly detection in practice [48]. With the detected node voltage $V_i(t)$ and the edge current $I_e(t)$, the complex power along the edge e is

$$S_{i,e}(t) = V_i(t) \cdot I_e(t)^*, \quad (7)$$

where $*$ is the complex conjugate. In two consecutive detections, we denote the change in power along the edge e detected by sensor i as $\Delta S_{i,e}(t)$.

2) *Anomaly Detector*: Anomaly can cause the voltage and current on one side to surge or decrease, thus producing complex effects on the entire grid. When one of the edges fails, the current will be redistributed among the edges of the grid as shown in Fig. 2 Part B. According to the current diversion, this redistribution leads to three anomaly patterns: single-edge anomaly, group anomaly, and group-diversion anomaly [8].

Based on the characteristics of the three types of anomalies, the corresponding three detectors are defined as follows:

- **Single-Edge Detector**: This detector focuses on the largest absolute change in power in the edges adjacent to a sensor v_i in the k -th time, i.e.,

$$x_{SE,i}(k) = \max_{e \in \mathcal{N}_i} |\Delta S_{i,e}(k)|. \quad (8)$$

- **Group Anomaly Detector**: This detector calculates the sum of all power changes in the edges adjacent to a sensor v_i , i.e.,

$$x_{GA,i}(k) = \left| \sum_{e \in \mathcal{N}_i} (\Delta S_{i,e}(k)) \right|. \quad (9)$$

- **Group-Diversion Detector**: The last detector computes the total absolute deviation of power changes about sensor v_i , i.e.,

$$x_{GD,i}(k) = \sum_{e \in \mathcal{N}_i} |\Delta S_{i,e}(k) - \text{mean}_{e' \in \mathcal{N}_i}(\Delta S_{i,e'}(k))|. \quad (10)$$

According to the results obtained by three detectors following Eqs. (8)-(10), we define the total slot detector in at time k as a vector $X_i(k) = [x_{SE,i}(k) \ x_{GA,i}(k) \ x_{GD,i}(k)]$, combining the outputs of three detectors simultaneously.

3) *Anomaly Score*: Based on the total detector result $X_i(k)$, we define an anomaly score to determine whether there is a fault in the grid. Considering sensor v_i and the total detector result $X_i(k)$, the anomaly score of this sensor in the k -th time can be computed via sensor-level anomalousness defined as follows [8]:

$$a_i(k) = \left\| \frac{X_i(k) - \tilde{\mu}_i(k)}{\tilde{\sigma}_i(k)} \right\|_{\infty}, \quad (11)$$

where $\tilde{\mu}_i(k)$ and $\tilde{\sigma}_i(k)$ are the historical median and inter-quartile range (IQR) [49] of $X_i(k)$, respectively; the infinity-norm $\|\cdot\|_{\infty}$ represents the maximum absolute value.

Moreover, considering only the abnormal score of one sensor measurement cannot reflect the overall abnormal situation since the power of the electrical grid changes dynamically with time. Thus, we define the overall anomaly score of a set of nodes $\mathcal{M} \subseteq \mathcal{V}$ as the maximum sensor-level anomaly score in \mathcal{M} , as follows:

$$A(k, \mathcal{M}) = \max_{v_i \in \mathcal{M}} a_i(k). \quad (12)$$

If the overall anomaly score exceeds a given threshold λ_a , i.e., $A(k, \mathcal{M}) > \lambda_a$, the sensors detected an anomaly within this time slot.

For a sensor placement performance evaluation, we need to consider its ability to detect abnormalities within a series of time slots. Specifically, suppose in a series of time $t_s = \{t_1, t_2, \dots, t_T\}$, s anomalies occurred at time $R_a = \{r_1, r_2, \dots, r_s\}$. For the set of nodes \mathcal{M} , the anomaly detection score S_a is

$$S_a(\mathcal{M}) = \frac{1}{s} \sum_{i=1}^s \mathbb{I}(A(r_i, \mathcal{M}) > \lambda_a), \quad (13)$$

where $\mathbb{I}(\cdot)$ is the indicator function, and λ_a is a given threshold.

IV. WIRELESS SENSOR PLACEMENT VIA GRAPH DIFFUSION POLICY OPTIMIZATION

In this section, we formulate the problem of robust wireless sensor placement in CPPS. We then introduce the EFGD policy optimization algorithm, which utilizes the diffusion framework for graph generation and optimizes policies through graph diffusion.

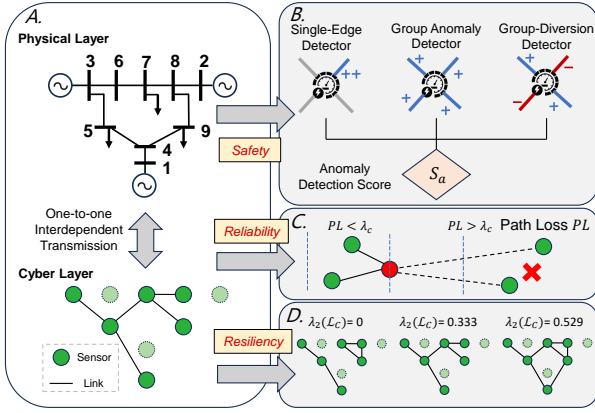


Fig. 2: The illustration of the optimization objections. *Part A.* The proposed CPPS system based on IEEE 9 bus system. *Part B.* The anomaly detectors focusing on the safety of the system. *Part C.* The communication quality based on LNSPL model targeting the reliability. *Part D.* The Fiedler value of different graphs addressing the robustness of the system.

A. Problem Formulation

According to the system model defined in Section III, we formulate the robust sensor placement problem considering both the physical layer layout and the cyber layer links simultaneously. Specifically, we aim to optimize a robust sensor placement $\mathcal{S} = (\mathcal{V}_S, \mathcal{E}_S)$, where $\mathcal{V}_S \subseteq \mathcal{V}$ consists of nodes to place sensors, and $\mathcal{E}_S \subseteq \mathcal{E}_C$ indicates the activated links. The objective is to maximize the accuracy of anomaly detection and ensure the network's robustness.

Specifically, the anomaly detection accuracy can be computed by the anomaly detection score S_a in Eq. (13). According to the LNSPL model in Eq. (1), the adjacency matrix E_C is composed of the communication state $l_{i,j}$ in Eq. (3) to guarantee the quality of communication when transmitting operation and control information. Additionally, the path loss in Eq. (1) varies over time due to shadowing. We assess the effectiveness of sensor placement under diffusion communication conditions to ensure robustness across different shadowing scenarios. Moreover, via maximizing the lower bound, the Fiedler value $\lambda_2(\mathcal{L}_S)$, computed by Eq. (6), we can approximate the Cheeger constant $h(\mathcal{L}_S)$, thereby ensuring the robustness of the communication network. In summary, our goal is to maximize the robustness of the cyber layer while ensuring accurate and effective anomaly detection of CPPS. Such a robust sensor placement problem can be formulated as:

$$\underset{\mathcal{S}}{\text{maximize}} \quad \lambda_2(\mathcal{L}_S) \quad (14a)$$

$$\text{s.t.} \quad S_a(\mathcal{V}_S) \geq \lambda_s, \quad (14b)$$

$$PL(v_i, v_j) \leq \lambda_c, \quad (v_i, v_j) \in \mathcal{E}_S, \quad (14c)$$

$$|\mathcal{V}_S| \leq N, \quad (14d)$$

where λ_s and λ_c are two given threshold values to ensure safety and reliability, respectively; N is the maximal number of sensors that can be placed. Although we approximate the

Cheeger constant to simplify the constraints, we have the following proposition regarding the NP-hardness of the above optimization problem.

Proposition 1. *The proposed robust sensor placement optimization problem (14) is NP-hard.*

Proof. To prove the NP-hardness of the proposed problem, we reduce the maximum algebraic connectivity augmentation problem, a well-known NP-hard problem [50], to the formulated problem. Specifically, for a given graph $\mathcal{G} = (\mathcal{V}, \mathcal{E})$ in the maximum algebraic connectivity augmentation problem, we set the anomaly score $S_a(\mathcal{V}) = \lambda_s$ and $S_a(\mathcal{V} - v_i) < \lambda_s$, $\forall v_i \in \mathcal{V}$, i.e., the constraint in Eq. (14b) is satisfied if and only if all vertices are selected. Moreover, we assign the weight of each edge in \mathcal{E} satisfying the constraint in Eq. (14c), while the edges not included in \mathcal{E} dissatisfy the constraint. Via this mapping, if we have an algorithm that can effectively solve the proposed robust sensor placement problem, it can solve the maximum algebraic connectivity augmentation problem. Therefore, the solution to the maximum algebraic connectivity augmentation problem can be derived through the solution of the proposed optimization problem (14). Since the maximum algebraic connectivity augmentation problem is NP-hard [50], the proposed optimization problem is NP-hard. \square

Solving NP-hard problems using traditional optimization methods is extremely challenging due to the significant computational resources and unpredictable solving times required. These methods often struggle with large and complex solution spaces that are not easily navigable using conventional techniques [16], where RL excels. Furthermore, diffusion-based RL algorithms can effectively explore the solution space through diffusion and denoising processes, allowing them to search for optimal strategies. These algorithms have demonstrated state-of-the-art performance, particularly in graph generation tasks [38]. Therefore, we present our proposed EFGD (Fig. 3) to solve such a graph generation problem.

B. Graph Diffusion

In this subsection, we will introduce the EFGD, which uses the generative diffusion model [34] to generate a solution graph for optimizing sensor placement.

1) *Discrete Diffusion Model:* Generative diffusion models, inspired by non-equilibrium thermodynamics, incorporate two Markov decision processes: forward diffusion and the denoising process, to generate new data [51]. In most of the diffusion models processing tasks, such as image generation, video generation, and audio generation, the data used in the two processes is generally continuous [35]. However, for graph generation problems, the data belongs to a discrete space, resulting in continuous noise that cannot be directly added. Therefore, in this paper, we use a discrete diffusion model to generate a sensor placement graph [52].

In the discrete diffusion model, the data state space \mathcal{Z} of the system is discrete. For an input data z , which has $|\mathcal{Z}|$ potential states, i.e., $|\mathcal{Z}|$ values, we process it by one-hot encoding. The one-hot encoded embedding can be denoted as $z \in \mathcal{Z}^{|\mathcal{Z}|}$.

Instead of adding random noise variables, the noises are represented by a series of transition matrices (Q^1, Q^2, \dots, Q^T) , where $[Q^t]_{i,j}$ denotes probability of changing from state $i \in \mathcal{Z}$ to state $j \in \mathcal{Z}$. Given an input z^0 , the prior distribution of a sequence of increasingly noisy data points z^1, z^2, \dots, z^T is

$$\begin{aligned} q(z^{1:T}|z^0) &= \prod_{t=1}^T q(z^t|z^{t-1}) \\ &= \prod_{t=1}^{T-1} q(z^t|z^{t-1}) \cdot Q^T \\ &= \dots \\ &= z^0 \cdot Q^1 Q^2 \dots Q^T, \end{aligned} \quad (15)$$

where $z^{1:T}$ represents the sequence z^1, z^2, \dots, z^T , $q(z^t|z^{t-1}) = z^{t-1} \cdot Q^t$ indicates the transition from state z^{t-1} to state z^t . Therefore, the distribution of noisy states z^t can be calculated directly by multiplying the transition matrix $q(z^t|z^0) = z^0 \cdot \bar{Q}^t$, where $\bar{Q}^t = Q^1 \dots Q^t$. Leveraging the Bayes rule, the posterior distribution $q(z^{t-1}|z^t, z^0)$ can be computed by [52]

$$q(z^{t-1}|z^t, z^0) \propto z^t (Q^t)' \odot z^0 \bar{Q}^{t-1}, \quad (16)$$

where \odot represents a pointwise product and Q' is the transpose of Q . Recall the goal of the original diffusion model is to transform an unknown distribution into a well-known one, such as a uniform distribution, via the forward diffusion process. Therefore, in the discrete diffusion model, we adopt the uniform transition matrix formulated as $Q^t = \alpha^t I + (1 - \alpha^t) \mathbf{1}_d \mathbf{1}'_d / d$ with α decreasing from 1 to 0. It can be proved that when $\lim_{t \rightarrow \infty} \alpha^t = 0$, $q(z^t|z^0)$ can coverage to a uniform distribution independently of z^0 with the uniform transition Q^t [53]. Then, we use a neural network to learn the posterior distribution $q(z^{t-1}|z^t, z^0)$, which can be utilized to recover the noisy data via the denoising process.

2) *Graph Forward Diffusion*: In our sensor placement optimization, we aim to generate an optimal sensor placement $\mathcal{S} = (\mathcal{V}_S, \mathcal{E}_S)$ represented by a graph tuple $G = (V, E)$, where V is vertices vector and E represents the corresponding adjacency matrix. Inspired by DiGress [54], we add noise incrementally for T steps to both the vertices vector V and the edge matrix E via the transition matrix. Based on the discrete diffusion model introduced above, we denote Q_V^t and Q_E^t as the t -th transition matrices for vertices and edges, respectively. For any vertices and edges, the transition probabilities are defined as $Q_V^t = q(v^t = j | v^{t-1} = i)$ and $Q_E^t = q(e^t = j | e^{t-1} = i)$. According to Eq. (15), given an input graph tuple $G^0 = (V^0, E^0)$, the forward diffusion process can be formulated as

$$q(G^{1:T}|G^0) = \prod_{t=1}^T q(G^t|G^{t-1}) = (V^0 \cdot \bar{Q}_V^T, E^0 \cdot \bar{Q}_E^T), \quad (17)$$

where \bar{Q}_V^t and \bar{Q}_E^t represent the product of the first t transition matrices of vertices and edges, respectively, and $G^{1:T}$ is the graph sequence G^1, G^2, \dots, G^T .

3) *Graph Denoising Process*: In general, the denoising process can be regarded as the reverse process of forward

diffusion, and its goal is to accurately estimate the posterior distribution for any initial input z^0 in Eq. (16). Consequently, the estimated posterior distribution p_θ can be expressed as [54]

$$\begin{aligned} p_\theta(G^{t-1}|G^t) \\ = \prod_{i=1}^n p_\theta(v_i^{t-1}|G^t) \prod_{1 \leq i, j \leq n} p_\theta(e_{ij}^{t-1}|G^t). \end{aligned} \quad (18)$$

For each term of vertices in Eq. (18), we can compute it by marginalization according to the initial state

$$\begin{aligned} p_\theta(v_i^{t-1}|G^t) &= \int_{v_i} p_\theta(v_i^{t-1}|v_i^0, G^t) dp_\theta(v_i|G^t) \\ &= \sum_{v \in \{0,1\}} p_\theta(v_i^{t-1}|v_i^0 = v, G^t) \hat{p}_i^V(v|G^t), \end{aligned} \quad (19)$$

where posterior distribution $\hat{p}_i^V(x)$ is a prediction based on $v \in \{0,1\}$ given a noisy graph G^t . Referring to Eq. (16), we let

$$p_\theta(v_i^{t-1}|v_i^0 = v, G^t) = q(v_i^{t-1}|v_i^0 = v, v_i^t). \quad (20)$$

Similarly, for each edge, we have

$$\begin{aligned} p_\theta(e_{ij}^{t-1}|e_{ij}^t) &= \sum_{e \in \{0,1\}} p_\theta(e_{ij}^{t-1}|e_{ij}^0 = e, G^t) \hat{p}_{ij}^E(e|G^t), \\ &= \sum_{e \in \{0,1\}} q(e_{ij}^{t-1}|e_{ij}^0 = e, e_{ij}^t) \hat{p}_{ij}^E(e|G^t). \end{aligned} \quad (21)$$

In summary, each denoising step can be formulated as [55]

$$p_\theta(G^{t-1}|G^t) = \sum_{G \in \mathcal{G}} q(G^{t-1}|G^0 = G, G^t) \hat{p}_\theta(G|G^t), \quad (22)$$

where \mathcal{G} denotes the set of all possible initial graphs, and $\hat{p}_\theta(G|G^t)$ is computed by a denoising network.

C. Experience Feedback Graph Diffusion Policy Gradient

Based on the forward diffusion and denoising process for graph generation, we can effectively learn the posterior distribution of graph data. However, for the sensor placement problem, we aim to obtain the posterior distribution of the optimal solution to the optimization (14). Inspired by GDPO [38], we model the denoising process as a T -step Markov decision process and solve it via RL. Given a Markov decision process $\mathcal{M} = (\mathcal{S}, \mathcal{A}, p_\theta, r, \rho_0)$, the proposed EFGD is defined as follows:

$$\begin{aligned} \mathbf{s}_t &\triangleq (G^{T-t}, T-t), \mathbf{a}_t \triangleq G^{T-t-1}, \\ \pi_\theta(\mathbf{a}_t|\mathbf{s}_t) &\triangleq p_\theta(G^{T-t-1}|G^{T-t}), \\ r(\mathbf{s}_t, \mathbf{a}_t) &\triangleq r(G^0), \text{ if } t = T, \\ r(\mathbf{s}_t, \mathbf{a}_t) &\triangleq 0, \text{ otherwise,} \end{aligned} \quad (24)$$

where $\mathbf{s}_t \in \mathcal{S}$ and $\mathbf{a}_t \in \mathcal{A}$ indicate the state and action at the t -th step respectively, π_θ represents the policy for sensor placement, p_θ is the transition function determining the probabilities of state transitions, $r(\mathbf{s}_t, \mathbf{a}_t)$ denotes the reward for action \mathbf{a}_t at state \mathbf{s}_t , ρ_0 gives the distribution of the initial noise graph state, and G^0 is the state after T -step denoising.

In the denoising process, as an agent interacts in the Markov decision process, we can acquire a trajectory denoted

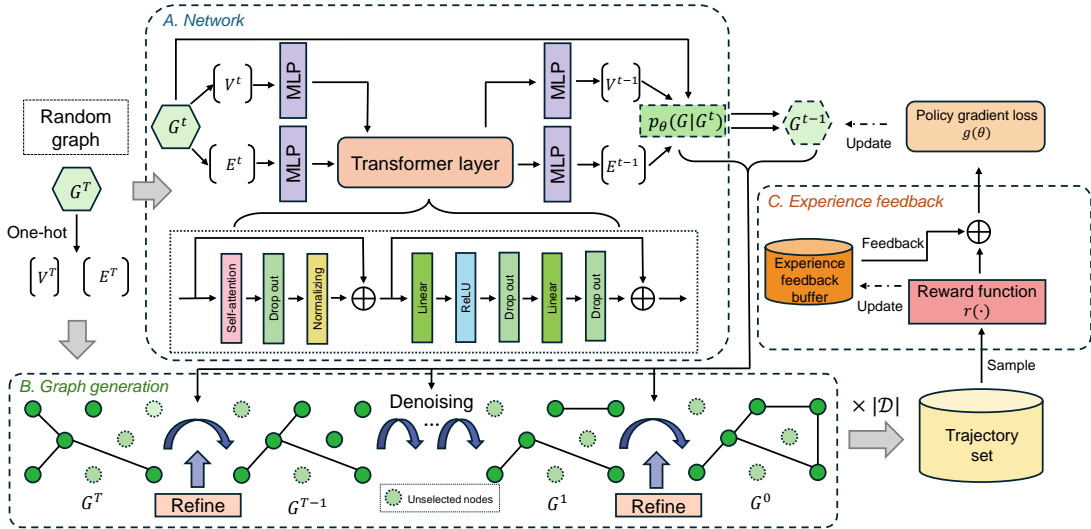


Fig. 3: The illustration of EFGD framework. *Part A.* The denoising network structure based on graph transformer architecture. *Part B.* The graph generation process based on the denoising graph diffusion model. *Part C.* The proposed experience feedback module.

as $\tau = (s_0, \mathbf{a}_0, s_1, \mathbf{a}_1, \dots, s_{T-1}, \mathbf{a}_{T-1}, s_T)$. The accumulative reward $R(\tau)$ of each trajectory is given by $R(\tau) = \sum_{t=0}^{T-1} r(s_t, \mathbf{a}_t) = r(G^0)$. To obtain an optimal sensor placement policy, the objective is to find a policy π_θ whose trajectory τ maximizes the expected accumulative reward $R(\tau)$, i.e.,

$$\mathcal{J}(\theta) = \mathbb{E}_{\tau \in p(\tau|\pi_\theta)}[R(\tau)] = \mathbb{E}_{G^0 \in p_\theta(G^{0:T})}[r(G^0)]. \quad (25)$$

We can notice that the expected accumulative reward $R(\tau)$ in Eq. (25) is equivalent to the expected reward of the final generated result. As a result, we can obtain the optimal sensor placement of the proposed optimization problem (14) via the denoising process. To effectively generate a policy trajectory, the EFGD can utilize the framework of policy gradient methods such as REINFORCE algorithm [56] and PPO algorithm [57]. Following the policy gradient, EFGD is trained to learn the optimal policy for the placement of wireless sensors. Given the objective $\mathcal{J}(\theta)$, the policy gradient $\nabla_\theta \mathcal{J}(\theta)$ can be expressed as

$$\begin{aligned} \nabla_\theta \mathcal{J}(\theta) &= \mathbb{E}_\tau [r(\mathbf{s}, \mathbf{a}) \nabla_\theta \log \pi_\theta(\mathbf{a}|\mathbf{s})] \\ &= \mathbb{E}_\tau \left[r(G^0) \sum_{t=0}^{T-1} \nabla_\theta \log p_\theta(G^{t-1}|G^t) \right]. \end{aligned} \quad (26)$$

However, when training based on the policy gradient in Eq. (26), the generated graph cannot converge to a high reward area due to the tremendous number of graph trajectories, particularly as the number of nodes increasing [58]. To solve this, we adopt the eager policy gradient in [38], which can be

written as

$$\nabla_\theta \mathcal{J}(\theta) = \mathbb{E}_\tau \left[r(G^0) \sum_{t=0}^{T-1} \nabla_\theta \log p_\theta(G^0|G^t) \right]. \quad (27)$$

In the eager policy gradient, the graph trajectories are partitioned into different equivalence classes based on the possible prior graph G^0 , where trajectories with the same G^0 are considered equivalent, thereby reducing the number of graph trajectories. Even though optimizing over these equivalence classes will be much easier than the original policy gradient to explore higher reward results, it still needs a certain convergence speed due to the slow convergence nature of diffusion [38].

To increase convergence speed, we improve the training process by modifying the policy gradient and the experience enhancement to eliminate fluctuating and unreliable policy gradient estimates.

1) *Cross-Entropy Gradient:* Inspired by the cross entropy loss, which is a measure of the difference between two probability distributions [59], we introduce a cross-entropy gradient, which can be expressed as

$$\nabla_\theta \mathcal{J}(\theta) = -\mathbb{E}_\tau \left[r(G^0) \sum_{t=0}^{T-1} \nabla_\theta (H(p_\theta(G^{0:T}), p_\theta(G^0|G^t))) \right], \quad (28)$$

where $H(p_\theta(G^{0:T}), p_\theta(G^0|G^t))$ is the cross entropy between the distribution of generated graph $p_\theta(G^{0:T})$ and the predicted distribution $p_\theta(G^0|G^t)$. Maximizing the cross-entropy gradient is equivalent to minimizing a reward-weighted cross-entropy function, thereby exploring higher rewards and making the

$$g(\theta) = \frac{1}{|\mathcal{D}|} \sum_{k=1}^{|\mathcal{D}|} \frac{T}{|\mathcal{T}_k|} \sum_{t \in \mathcal{T}_k} \left(\frac{r(G_k^0) - \mu_r}{\sigma_r} H(p_\theta(G_k^{0:T}), p_\theta(G_k^0|G_k^t)) + \beta \cdot H(p(\tilde{G}_k), p_\theta(G_k^0|G_k^t)) \right). \quad (23)$$

predicted distribution closer to the final distribution.

2) *Trajectory Experience Feedback*: Based on the RLHF, which selects the highest reward strategy as the experience feedback, we propose a trajectory experience feedback to accelerate training convergence. Different from the experience replay, the experience feedback is a generated graph with the highest reward rather than a series of action policies. Letting $p(\tilde{G})$ as the distribution of the experience graph, the loss function can be written as

$$l_{CEM} = \mathbb{E}_\tau \left[\mathbb{E}_t [H(p(\tilde{G}), p_\theta(G^0|G^t))] \right]. \quad (29)$$

To minimize the loss function l_{CEM} , the network can use optimization solutions with higher rewards, thereby accelerating the training and convergence of the network. In practice, we select the experience graph \tilde{G} from an experience feedback buffer \mathcal{B} consisting of $|\mathcal{B}|$ trajectories with the highest reward by comparing the mean square error with the current prediction G^0 .

Combining the proposed two training strategies together, we approximate Eqs. (28) and (29) with a Monte Carlo estimation to obtain the loss function. Moreover, we adopt reward standardization in the training stage to ensure the stability and convergence of network training. The standardized loss function can be written as Eq. (23), where \mathcal{D} and \mathcal{T}_k represent the sets of sampled trajectories and timesteps, respectively, μ_r and σ_r represent the mean value and variance of the reward for each action on the collected trajectory, respectively, and β is an adjustable weight parameter.

In summary, the proposed EFGD method aims to train a neural network p_θ to learn the posterior distribution in Eq. (18). Via formulating the denoising process as a T -step Markov decision process \mathcal{M} , we use the policy gradient framework to train the network p_θ with the modified loss function as Eq. (23) to ensure the stability and convergence of network training. Then, the parameter θ of the network p_θ is updated by stochastic gradient descent. Finally, we sample the Markov decision process trajectories using the trained network p_θ via denoising process in Eq. (22).

D. EFGD for Wireless Sensor Placement

In this subsection, we show the data flow processing in different procedures and present our EFGD framework for wireless sensor placement. Moreover, we outline the deployment details of EFGD for optimization, including reward function setting, network structure, and optimization process.

The entire EFGD process is detailed in Algorithm 1 and illustrated in Fig. 3. We aim to train a denoising network capable of estimating the posterior distribution. Each training epoch begins with the random generation of initially noised graphs. Subsequently, \mathcal{D} trajectories are produced to form the trajectory set \mathcal{D} , originating from the initial graphs as depicted in Figure 3 *Part B*. During the denoising process, a refinement operation is applied to validate the generated edge matrix, ensuring its symmetry and the connectivity of only selected points. Graph trajectories are then sampled, and their rewards are calculated based on the reward function $r(\cdot)$. Particularly, during the reward calculation process, the

refinement operation eliminates the edges that do not meet the constraint in Eq. (14c) to validate the generated sensor placement strategy. Moreover, an experience feedback buffer is maintained, which stores the higher reward trajectories. We select the most suitable trajectory experience feedback based on the minimum mean square error (MMSE) between the two graphs. This feedback, along with the trajectories, is then used to compute the policy gradient loss in Eq. (23) to train the denoising network.

1) *Reward Function Setting*: Recall our goal is to utilize EFGD to solve the optimization problem (14) and obtain the optimal sensor emplacement policy. Achieving this objective requires an appropriate reward function r for graph generation in the Markov decision process \mathcal{M} . Considering both the optimized objective and constraints in the optimization problem, we define a penalty-constrained reward function whose penalty terms are the constraints [60]. Specifically, the penalty-constrained reward function r can be expressed as

$$r(G^0) = \begin{cases} r_1 \cdot \lambda_2(\mathcal{L}_{G^0}), & \text{if } I_1 \times I_2 = 1, \\ -r_2 \cdot (|\mathcal{V}_{G^0}| - N) - r_3 \cdot (\lambda_s - S_a(\mathcal{V}_{G^0})), & \text{otherwise,} \end{cases} \quad (30)$$

where $I_1 = \mathbf{1}(|\mathcal{V}_{G^0}| \leq N)$ and $I_2 = \mathbf{1}(S_a \leq \lambda_s)$; $\mathbf{1}$ denote the indicator; r_1 , r_2 , and r_3 are adjustable weight ratio. Based on the penalty terms, an agent in the Markov decision process \mathcal{M} can obtain a non-zero reward only if the sensor placement policy generated by the chosen action satisfies the constraints. Additionally, due to the different magnitudes of different conditions, we use adjustable weight ratios r_i to ensure learning capabilities for different constraints. Consequently, for a Markov decision process \mathcal{M} and the penalty-constrained reward function r , the denoising result following the trajectory of the maximum cumulative reward will correspond to the optimal solution of the optimization problem (14), i.e., the optimal robust sensor placement policy.

2) *Network Structure*: We construct the denoising network for EFGD via the graph transformer architecture based on [38] as shown in Fig. 3 *Part A*. Firstly, one-hot embeddings of nodes and edges are extracted from the graph G^t , respectively, to convert state information into probability space to facilitate prediction of node and edge selection. These embeddings are then mapped to latent space through the Multi-layer Perception (MLP) layer, which consists of a combination of two consecutive linear layers and Rectified Linear Unit (ReLU) activation functions. Subsequently, the processed node and edge data are input into a transformer structure together, using a self-attention mechanism based on a Feature-wise Linear Modulation layer [38] to focus on each detail feature. Simultaneously, the dropout layer is utilized to prevent the network from being overfitted. Residual connections and normalizing layers are combined to facilitate network learning, enhance stability, and prevent gradient explosion and disappearance. Finally, the MLP layer is used to restore the original probability space $p_\theta(G|G^t)$ to predict the current selection of the edges and nodes G^{t-1} .

Algorithm 1: The proposed EFGD algorithm

Input: Initial denoising network p_θ , a Markov decision process $\mathcal{M} = (\mathcal{S}, \mathcal{A}, p_\theta, r, \rho_0)$, # of denoising steps T , # of trajectory sample $|\mathcal{D}|$, # of timestep samples $|\mathcal{T}|$, learning rate γ , # of training steps N_t , # of the size of experience feedback buffer $|\mathcal{B}|$;

Procedure 1: EFGD Training;

```

for  $i = 1, 2, \dots, N_t$  do
  for  $d = 1, 2, \dots, |\mathcal{D}|$  do
    Sample initial noisy graph from the Markov
    decision process  $\mathcal{M}$ 
    for  $t = 1, 2, \dots, T$  do
      | Perform denoising based on Eq. (22)
    end
    Acquire trajectory  $\tau_d$ 
    Sample timestep  $T_d \sim \text{Uniform}([1, T])$ 
    Calculate reward  $r(G^0)$  based on Eq. (30)
    Update experience feedback buffer  $\mathcal{B}$  based on the
    reward  $r(G^0)$ 
  end
end
  Calculate policy gradient loss  $g(\theta)$  based on Eq. (23)
  Update  $p_\theta$  parameters by gradient descent

```

Procedure 2: EFGD Inference;

```

for  $t = 1, 2, \dots, T$  do
  | Perform denoising process based on Eq. (22)
end

```

Output: Generated sensor placement G^0

V. NUMERICAL RESULTS

In this section, we implement the proposed sensor placement problem in a real power system, IEEE 118-Bus System [61]. Then, we conduct extensive experiments to evaluate the proposed EFGD algorithm, covering two aspects: algorithm performance and the impact of hyperparameters on performance.

A. Experiment Setting

The experiments are conducted on a Linux server with an NVIDIA A100 GPU with 80 GB of memory. All codes are written in Python, network training is based on the PyTorch package, and power grid simulation uses the pypower package [61]. Due to the sensor placement problem, we cannot get real-time monitoring data from sensors. Therefore, we generate a dataset of anomalies and normal scenarios in the IEEE 118-Bus System through the pypower simulator with the same power load setting in [8]. By considering resistance information as distance information, we utilize Multidimensional Scaling [62] to simulate the 2D coordinates of the nodes in the power grid. Then, we can calculate the distance between any two nodes via 2D coordinates. For the LNSPL model, we utilize the parameters of a smart grid substation model with IEEE 802.15.4 [42]. Specifically, the reference distance d_0 is 1m, the reference path loss is set at 40.3308 dB, the path loss exponent γ is 1.701, and the variance σ of the Gaussian noise X_σ is set at 2.18 dB. Furthermore, we set that the transmission power is 10 dBm, the noise power is -90 dBm, and the signal-to-noise ratio in Eq. (2) must exceed 25 dB to ensure a lower transmission error [63]. Therefore, the links whose path loss between nodes is greater than 75 dB are unstable and may

fail, which establishes the threshold λ_c in Eq. (14c) as 75 dB. For anomaly detection, we assume that the budget cap for the number of sensors is 25, i.e., $N = 25$ in Eq. (14d). The threshold λ_a for the anomaly detection score S_a is set at 50. Additionally, the accuracy of the detection is 90%, which sets $\lambda_s = 0.90$ in Eq. (14b). For training, we set all methods' batch size and learning rate to 256 and 1×10^{-5} , respectively. Then, we train each learning method for 90 epochs, with the reward function and network structure discussed in Subsection IV-D. The weight ratios are set as $r_1 = 5000$, $r_2 = 1.075$, and $r_3 = 0.5$.

B. Performance Comparison

1) *Baseline Methods:* We benchmark the proposed EFGD algorithm with the following baselines: **Greedy-Accuracy**, where the greedy strategy based on GridWatch is adopted to ensure the accuracy of anomaly detection [8]; **Greedy-Robustness**, where the greedy algorithm identifies the optimal location and link connection for the new node by iteration, aiming to maximize the Fiedler value of sensor placement; **Random**, where the sensor placement nodes and network connections are randomly selected; **GDPO**, which follows the graph diffusion optimization framework in [38]; **DDPO**, which is a deep RL algorithm based on standard negative log policy gradient [58]. Note that the RL baselines, including GDPO and DDPO, are set to the same setting as the proposed method EFGD. Additionally, for the proposed method EFGD, the diffusion step is 20, the buffer length is 50, and the weight parameter $\beta = 0.2$.

2) *Sensor Placement Optimization:* Fig. 4 illustrates the average reward (denoted as AvgReward) achieved by the EFGD and compared to the baseline learning methods DDPO and GDPO, where EFGD, DDPO, and GDPO reward curves are represented in red, orange, and yellow, respectively. Initially, when the condition $I_1 \times I_2 = 1$ in the reward function (Eq. (30)) is mostly unsatisfied, indicating the phase where the models are learning the constraints, the performances of all three methods are comparable, with GDPO slightly outperforming the others. As the training progresses beyond the constraint learning phase and into the objective function learning phase, where the models start generating graphs that satisfy the constraints around 40 epochs, there is a significant reward improvement in all models compared to their initial performances with the increment in positive samples. Moreover, the average reward for the EFGD strategy shows a remarkable increase compared to the other two benchmarks. Notably, EFGD converges after 60 epochs, while DDPO and GDPO take approximately 74 epochs. This observation underscores that additional experience feedback can effectively enhance the model's convergence speed by 18.9%. Comparing the average AvgReward since the convergence epoch, EFGD reaches an average AvgReward of 2.2007, while DDPO and GDPO converge with an average reward of -9.9470 and -8.4694, respectively. With -63 as the baseline average starting reward, the proposed EFGD algorithm can enhance the average reward by 22.90% compared to DDPO, and by 19.57% compared to GDPO.

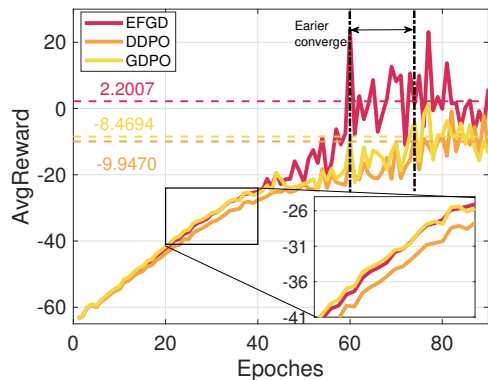


Fig. 4: The average reward (AvgReward) of EFGD and other baselines over training epochs.

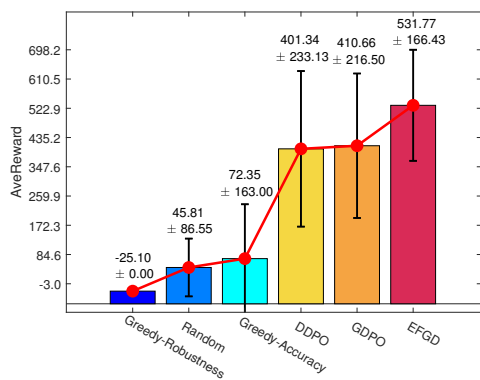


Fig. 5: The average reward (AvgReward) of EFGD and other baselines in the inference stage.

Further analysis is conducted using these aforementioned algorithms to generate 50 sensor placement strategies, evaluating the average reward and variance of these strategies under 100 test conditions. The results for the optimal placement strategy for each method are plotted in Fig. 5. The traditional baseline methods show a stark contrast in performance: Greedy-Robustness scores the lowest at -25.10 ± 0.00 , Greedy-Accuracy has a performance of 72.35 ± 163.00 , and Random strategy yields 45.81 ± 86.55 . In comparison, the RL-based methods significantly outperformed these, with DDPO achieving 401.34 ± 233.13 , GDPO 410.66 ± 216.50 , and EFGD excelling at 531.77 ± 166.43 . The results highlight that the proposed EFGD surpasses the learning baselines GDPO and DDPO by 25.57% and 28.09%, respectively, and outperforms traditional methods by over 400%. The primary reason why the performance of the two greedy algorithms is similar to that of the random algorithm yet significantly lower than that of the learning-based method is that each greedy algorithm focuses solely on one aspect of the system, such as accuracy or robustness. This narrow focus makes it challenging to meet the overall constraints of the optimization or to fully maximize the optimization goal, thereby demonstrating that traditional methods are inadequate for such complex NP-hard challenges. Furthermore, the substantial improvement

over other learning underscores the efficacy of incorporating high-reward strategies as experience feedback into the model, which enables a sharper focus on such strategies and facilitates convergence to more optimal solutions. Moreover, the reduced standard deviation of the reward from the generated placement policy indicates that the sensor placement produced by EFGD exhibits more robust performance across varying conditions.

Fig. 6 illustrates the graph generation process of the trained EFGD model under varying communication conditions. The displayed results confirm that EFGD adeptly adjusts its node and edge generation processes during the denoising process. This capability enables the generation of graphs that effectively meet the requirements imposed by diverse scenarios, thereby demonstrating the model’s extensive generalizability. Moreover, it is noteworthy that in the generated graphs, nodes are interconnected by multiple edges. This structural characteristic significantly enhances the robustness of the network, ensuring that the graph remains connected even in the event of edge failures. Such robustness is critical in maintaining the integrity and operational stability of the system under adverse conditions.

C. Hyperparameters Analysis

Next, we analyze the impact of model hyperparameters on the performance of the proposed model from three aspects, including 1). the number of diffusion steps T ; 2). the value of weight parameter β ; and 3). the size of experience feedback buffer $|\mathcal{B}|$.

1) *Diffusion Step*: First, our analysis focuses on the impact of the diffusion step size on the reward achieved by the model’s generation strategy. The diffusion step size generally influences the generation quality of diffusion models. A longer step size typically pushes the noise-added distribution closer to the standard normal distribution, facilitating the learning of an accurate posterior distribution. As depicted in Fig. 7, the diffusion step labeled as “EFGD- T ” varies, where “ T ” represents the number of diffusion steps. With the exception of “EFGD-5”, which shows a slower convergence, the trends of the other three curves (“EFGD-10”, “EFGD-20”, “EFGD-30”) are remarkably similar, all converging within 60 epochs. Furthermore, The average AvgRewards post-convergence are as follows: EFGD-5: -6.9043 ; EFGD-10: 2.0901 ; EFGD-20: 2.2007 ; EFGD-30: -0.4780 . These results indicate that there is generally an upward trend in the reward as the noise addition step length increases. However, performance declines when the diffusion step length becomes excessively large. This decline can be attributed to the fact that the final denoising result, G^0 , is used as the trajectory’s reward and the basis for calculating the policy gradient. While this approach emphasizes the overall scenario, it overlooks the finer details, particularly the reward attributed to each step. As the diffusion step length increases, the exploration capabilities of the model are somewhat diminished, thereby adversely affecting performance. In summary, we need to select an appropriate de-noising step size to balance details and global features.

2) *Weight Parameter*: We then investigate the effect of the weight parameter β on model performance, which modulates

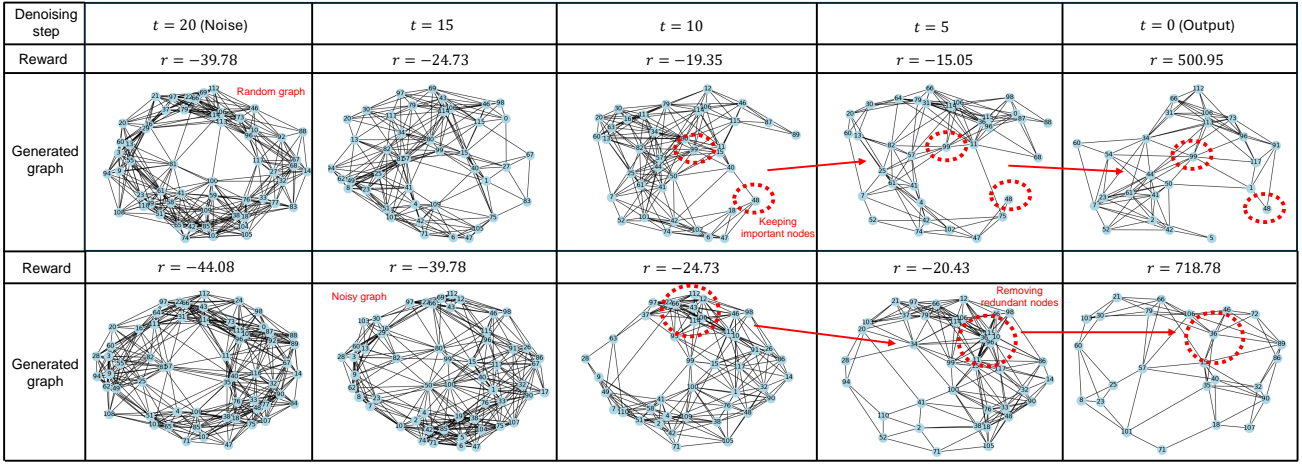


Fig. 6: The illustration of the graph generation process in IEEE-118 bus system under two communication conditions.

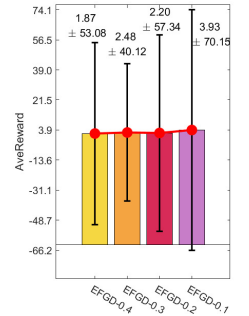
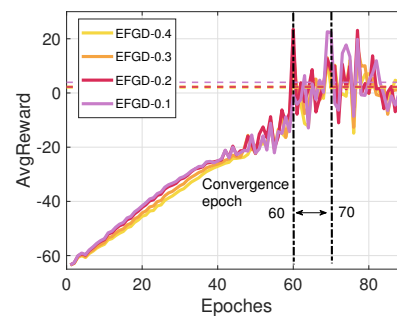
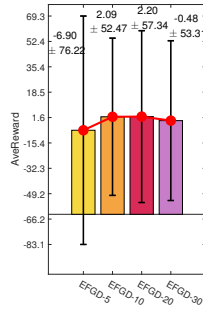
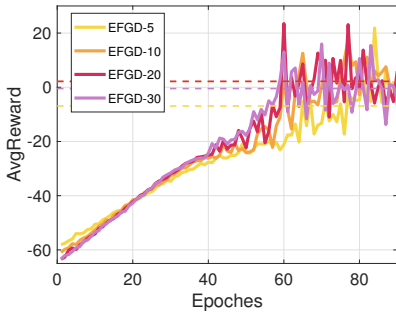


Fig. 7: The average reward (AvgReward) of EFGD under different diffusion steps.

Fig. 8: The average reward (AvgReward) of EFGD under different weight parameters.

the influence of experience feedback on the current policy gradient. As this parameter increases, so does the impact of the feedback on the gradient calculations. Fig. 8 presents the convergence behavior of the model at various weights. At a β value of 0.1, the model “EFGD-0.1” converges at 70 epochs, demonstrating a faster convergence than the original 74 epochs observed for GDPO and DDPO. As the weight parameter increases further, the convergence consistently occurs around 60 epochs. Upon examining the average AvgReward after convergence, a trend emerges where the average reward decreases as the weight parameter increases. Specifically, The average rewards for EFGD with parameters -0.1, -0.2, -0.3, and -0.4 are as follows: 3.9522, 2.2007, 2.4789, and 1.8746, respectively. The performance of “EFGD-0.4” is 3% lower than that of “EFGD-0.1”. This decrement in performance suggests that with higher feedback weights, the model increasingly focuses on previously explored strategies. This shift in focus can reduce the model’s capability to explore new strategies, potentially leading to premature convergence to local optima and, thus, a decline in overall performance.

3) *Size of Experience Feedback Buffer*: Lastly, we evaluate the role of the experience feedback buffer size in shaping model performance. An increase in buffer size allows the storage of a larger number of previously successful strategies, which the model utilizes as references when calculating the

policy gradient using the MMSE as a similarity criterion. Fig. 9 illustrates that regardless of buffer size, all variations of the model converge around 60 epochs. Furthermore, the average AvgReward after convergence demonstrates that within a certain range, an increase in buffer size enhances model performance. Specifically, with buffer sizes of 10, 20, and 50, the AvgRewards are 1.7152, 1.8329, and 2.2007, respectively. Conversely, an excessively large buffer size, such as 1000, results in a significant reduction in performance, with an average AvgReward of 0.1120. This decrease in performance with larger buffer sizes can be attributed to the buffer’s capacity to accumulate many local optimal strategies that are not effectively replaced through trajectory sampling. As a result, many trajectories may rely excessively on these suboptimal strategies as feedback, thereby predisposing the model towards local optima. Thus, while an increased buffer size can facilitate faster convergence and initially improve performance by providing richer experiential feedback, there is a critical balance to be maintained. It is vital to optimize the buffer size to ensure a diversity of optimal solutions and mitigate the dominance of local optima, thus maintaining the efficacy and generalizability of the model.

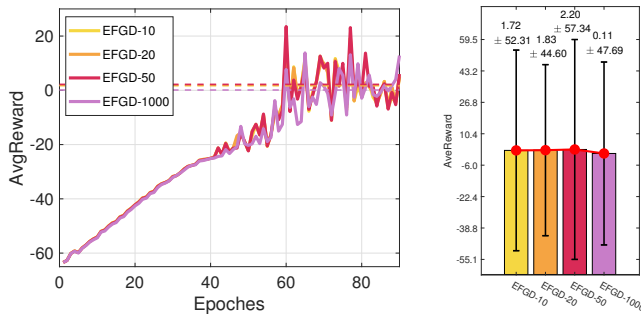


Fig. 9: The average reward (AvgReward) of EFGD under different sizes of experience feedback buffer.

VI. CONCLUSION

In this work, we have presented a novel approach for optimizing robust sensor placement within CPPS. Our approach involved modeling the sensor placement challenge as a graph-based optimization problem, utilizing the LNSPL model to ensure reliable data transmission, the Fiedler value to assess graph robustness against line failures, and employing three anomaly detectors to enhance system safety. We first proved the proposed optimization problem is NP-hard. To address this complex optimization, we have proposed the EFGD algorithm, which employs a graph diffusion model integrated with cross-entropy gradient and experience feedback mechanisms. By combining the experience feedback, the proposed EFGD can converge faster to find a better solution with higher rewards tailored to effectively solve the robust sensor placement optimization problem. Several simulation results show that EFGD outperforms traditional methods in optimizing sensor placements, thus ensuring robust and reliable CPPS operations.

REFERENCES

- [1] X. Fang, S. Misra, G. Xue, and D. Yang, "Smart grid—the new and improved power grid: A survey," *IEEE communications surveys & tutorials*, vol. 14, no. 4, pp. 944–980, 2011.
- [2] S. Sridhar, A. Hahn, and M. Govindarasu, "Cyber-physical system security for the electric power grid," *Proceedings of the IEEE*, vol. 100, no. 1, pp. 210–224, 2011.
- [3] R. V. Yohanandhan, R. M. Elavarasan, P. Manoharan, and L. Mihet-Popa, "Cyber-physical power system (cpps): A review on modeling, simulation, and analysis with cyber security applications," *IEEE Access*, vol. 8, pp. 151 019–151 064, 2020.
- [4] X. Huang, T. Han, and N. Ansari, "Smart grid enabled mobile networks: Jointly optimizing bs operation and power distribution," *IEEE/ACM Transactions on Networking*, vol. 25, no. 3, pp. 1832–1845, 2017.
- [5] X. Lyu, Y. Ding, and S.-H. Yang, "Safety and security risk assessment in cyber-physical systems," *IET Cyber-Physical Systems: Theory & Applications*, vol. 4, no. 3, pp. 221–232, 2019.
- [6] S. Li, A. Pandey, B. Hooi, C. Faloutsos, and L. Pileggi, "Dynamic graph-based anomaly detection in the electrical grid," *IEEE Transactions on Power Systems*, vol. 37, no. 5, pp. 3408–3422, 2021.
- [7] X. Niu, J. Li, J. Sun, and K. Tomsovic, "Dynamic detection of false data injection attack in smart grid using deep learning," in *2019 IEEE Power & Energy Society Innovative Smart Grid Technologies Conference (ISGT)*. IEEE, 2019, pp. 1–6.
- [8] B. Hooi, D. Eswaran, H. A. Song, A. Pandey, M. Jereminov, L. Pileggi, and C. Faloutsos, "Gridwatch: Sensor placement and anomaly detection in the electrical grid," in *Machine Learning and Knowledge Discovery in Databases: European Conference, ECML PKDD 2018, Dublin, Ireland, September 10–14, 2018, Proceedings, Part I 18*. Springer, 2019, pp. 71–86.
- [9] C. M. Schneider, A. A. Moreira, J. S. Andrade Jr, S. Havlin, and H. J. Herrmann, "Mitigation of malicious attacks on networks," *Proceedings of the National Academy of Sciences*, vol. 108, no. 10, pp. 3838–3841, 2011.
- [10] T. Qiu, A. Zhao, F. Xia, W. Si, and D. O. Wu, "Rose: Robustness strategy for scale-free wireless sensor networks," *IEEE/ACM Transactions on Networking*, vol. 25, no. 5, pp. 2944–2959, 2017.
- [11] H. Zhang, E. Fata, and S. Sundaram, "A notion of robustness in complex networks," *IEEE Transactions on Control of Network Systems*, vol. 2, no. 3, pp. 310–320, 2015.
- [12] X. Xu, X.-Y. Li, and M. Song, "Efficient aggregation scheduling in multi-hop wireless sensor networks with sinr constraints," *IEEE transactions on mobile computing*, vol. 12, no. 12, pp. 2518–2528, 2012.
- [13] E. Clark, T. Askham, S. L. Brunton, and J. N. Kutz, "Greedy sensor placement with cost constraints," *IEEE sensors journal*, vol. 19, no. 7, pp. 2642–2656, 2018.
- [14] G. Wu and Z. S. Li, "Cyber-physical power system (cpps): a review on measures and optimization methods of system resilience," *Frontiers of Engineering Management*, vol. 8, no. 4, pp. 503–518, 2021.
- [15] N. M. M. De Abreu, "Old and new results on algebraic connectivity of graphs," *Linear algebra and its applications*, vol. 423, no. 1, pp. 53–73, 2007.
- [16] Y. Li, "Deep reinforcement learning: An overview," *arXiv preprint arXiv:1701.07274*, 2017.
- [17] H. Du, R. Zhang, Y. Liu, J. Wang, Y. Lin, Z. Li, D. Niyato, J. Kang, Z. Xiong, S. Cui *et al.*, "Enhancing deep reinforcement learning: A tutorial on generative diffusion models in network optimization," *IEEE Communications Surveys & Tutorials*, 2024.
- [18] H. Du, R. Zhang, D. Niyato, J. Kang, Z. Xiong, and D. I. Kim, "Reinforcement learning with large language models (llms) interaction for network services," *Authorea Preprints*, 2024.
- [19] P.-Y. Kong, "Routing in communication networks with interdependent power grid," *IEEE/ACM Transactions on Networking*, vol. 28, no. 4, pp. 1899–1911, 2020.
- [20] E. Keogh, J. Lin, S.-H. Lee, and H. V. Herle, "Finding the most unusual time series subsequence: algorithms and applications," *Knowledge and Information Systems*, vol. 11, pp. 1–27, 2007.
- [21] S. Yi, J. Ju, M.-K. Yoon, and J. Choi, "Grouped convolutional neural networks for multivariate time series," *arXiv preprint arXiv:1703.09938*, 2017.
- [22] J. Yang, B. Delinchant, D. Niyato, and N. Hadjsaid, "Hybrid model of convolutional auto-encoder and ellipse characteristic for unsupervised high impedance fault detection," *Electric Power Systems Research*, vol. 238, p. 111166, 2025.
- [23] S. Ramaswamy, R. Rastogi, and K. Shim, "Efficient algorithms for mining outliers from large data sets," in *Proceedings of the 2000 ACM SIGMOD international conference on Management of data*, 2000, pp. 427–438.
- [24] F. T. Liu, K. M. Ting, and Z.-H. Zhou, "Isolation forest," in *2008 eighth IEEE international conference on data mining*. IEEE, 2008, pp. 413–422.
- [25] L. Akoglu, M. McGlohon, and C. Faloutsos, "Oddball: Spotting anomalies in weighted graphs," in *Advances in Knowledge Discovery and Data Mining: 14th Pacific-Asia Conference, PAKDD 2010, Hyderabad, India, June 21–24, 2010. Proceedings. Part II 14*. Springer, 2010, pp. 410–421.
- [26] Z. Chen, W. Hendrix, and N. F. Samatova, "Community-based anomaly detection in evolutionary networks," *Journal of Intelligent Information Systems*, vol. 39, no. 1, pp. 59–85, 2012.
- [27] L. Akoglu and C. Faloutsos, "Event detection in time series of mobile communication graphs," in *Army science conference*, vol. 1, 2010, p. 141.
- [28] C. C. Aggarwal, Y. Zhao, and S. Y. Philip, "Outlier detection in graph streams," in *2011 IEEE 27th international conference on data engineering*. IEEE, 2011, pp. 399–409.
- [29] S. Ranshous, S. Harenberg, K. Sharma, and N. F. Samatova, "A scalable approach for outlier detection in edge streams using sketch-based approximations," in *Proceedings of the 2016 SIAM international conference on data mining*. SIAM, 2016, pp. 189–197.
- [30] Q. Li, R. Negi, and M. D. Ilić, "Phasor measurement units placement for power system state estimation: A greedy approach," in *2011 IEEE power and energy society general meeting*. IEEE, 2011, pp. 1–8.
- [31] A. M. Koster, M. Kutschka, and C. Raack, "Robust network design: Formulations, valid inequalities, and computations," *Networks*, vol. 61, no. 2, pp. 128–149, 2013.
- [32] T. Qiu, J. Liu, W. Si, and D. O. Wu, "Robustness optimization scheme with multi-population co-evolution for scale-free wireless sensor networks," *IEEE/ACM Transactions on Networking*, vol. 27, no. 3, pp. 1028–1042, 2019.

- [33] G. Egeland and P. E. Engelstad, "The availability and reliability of wireless multi-hop networks with stochastic link failures," *IEEE Journal on Selected Areas in Communications*, vol. 27, no. 7, pp. 1132–1146, 2009.
- [34] J. Ho, A. Jain, and P. Abbeel, "Denoising diffusion probabilistic models," *Advances in neural information processing systems*, vol. 33, pp. 6840–6851, 2020.
- [35] L. Yang, Z. Zhang, Y. Song, S. Hong, R. Xu, Y. Zhao, W. Zhang, B. Cui, and M.-H. Yang, "Diffusion models: A comprehensive survey of methods and applications," *ACM Computing Surveys*, vol. 56, no. 4, pp. 1–39, 2023.
- [36] J. Wang, H. Du, Y. Liu, G. Sun, D. Niyato, S. Mao, D. I. Kim, and X. Shen, "Generative ai based secure wireless sensing for isac networks," *arXiv preprint arXiv:2408.11398*, 2024.
- [37] C. Zhao, H. Du, D. Niyato, J. Kang, Z. Xiong, D. I. Kim, X. Shen, and K. B. Letaief, "Generative ai for secure physical layer communications: A survey," *IEEE Transactions on Cognitive Communications and Networking*, 2024.
- [38] Y. Liu, C. Du, T. Pang, C. Li, W. Chen, and M. Lin, "Graph diffusion policy optimization," *arXiv preprint arXiv:2402.16302*, 2024.
- [39] J. Wang, Y. Liu, H. Du, D. Niyato, J. Kang, H. Zhou, and D. I. Kim, "Empowering wireless networks with artificial intelligence generated graph," *arXiv preprint arXiv:2405.04907*, 2024.
- [40] M. Vecerik, T. Hester, J. Scholz, F. Wang, O. Pietquin, B. Piot, N. Heess, T. Rothörl, T. Lampe, and M. Riedmiller, "Leveraging demonstrations for deep reinforcement learning on robotics problems with sparse rewards," *arXiv preprint arXiv:1707.08817*, 2017.
- [41] S. Kurt and B. Tavli, "Path-loss modeling for wireless sensor networks: A review of models and comparative evaluations," *IEEE Antennas and Propagation Magazine*, vol. 59, no. 1, pp. 18–37, 2017.
- [42] R. M. Sandoval, A.-J. Garcia-Sanchez, and J. Garcia-Haro, "Improving rssi-based path-loss models accuracy for critical infrastructures: A smart grid substation case-study," *IEEE Transactions on Industrial Informatics*, vol. 14, no. 5, pp. 2230–2240, 2017.
- [43] X. Liu, D. Li, M. Ma, B. K. Szymanski, H. E. Stanley, and J. Gao, "Network resilience," *Physics Reports*, vol. 971, pp. 1–108, 2022.
- [44] B. Mohar, "Isoperimetric numbers of graphs," *Journal of combinatorial theory, Series B*, vol. 47, no. 3, pp. 274–291, 1989.
- [45] F. R. Chung, *Spectral graph theory*. American Mathematical Soc., 1997, vol. 92.
- [46] Y. Yoshida, "Cheeger inequalities for submodular transformations," in *Proceedings of the Thirtieth Annual ACM-SIAM Symposium on Discrete Algorithms*. SIAM, 2019, pp. 2582–2601.
- [47] B. Eiteneuer, N. Hranisavljevic, and O. Niggemann, "Dimensionality reduction and anomaly detection for cpps data using autoencoder," in *2019 IEEE International Conference on Industrial Technology (ICIT)*. IEEE, 2019, pp. 1286–1292.
- [48] S. Park and A. Pandey, "Anomaly detection in power grids via context-agnostic learning," *arXiv preprint arXiv:2404.07898*, 2024.
- [49] G. U. Yule, *An introduction to the theory of statistics*. C. Griffin, 1927.
- [50] D. Mosk-Aoyama, "Maximum algebraic connectivity augmentation is np-hard," *Operations Research Letters*, vol. 36, no. 6, pp. 677–679, 2008.
- [51] H. Cao, C. Tan, Z. Gao, Y. Xu, G. Chen, P.-A. Heng, and S. Z. Li, "A survey on generative diffusion models," *IEEE Transactions on Knowledge and Data Engineering*, 2024.
- [52] J. Austin, D. D. Johnson, J. Ho, D. Tarlow, and R. Van Den Berg, "Structured denoising diffusion models in discrete state-spaces," *Advances in Neural Information Processing Systems*, vol. 34, pp. 17981–17993, 2021.
- [53] D. Yang, J. Yu, H. Wang, W. Wang, C. Weng, Y. Zou, and D. Yu, "Diffsound: Discrete diffusion model for text-to-sound generation," *IEEE/ACM Transactions on Audio, Speech, and Language Processing*, vol. 31, pp. 1720–1733, 2023.
- [54] C. Vignac, I. Krawczuk, A. Siraudin, B. Wang, V. Cevher, and P. Frossard, "Digress: Discrete denoising diffusion for graph generation," *arXiv preprint arXiv:2209.14734*, 2022.
- [55] T. Karras, M. Aittala, T. Aila, and S. Laine, "Elucidating the design space of diffusion-based generative models," *Advances in neural information processing systems*, vol. 35, pp. 26565–26577, 2022.
- [56] R. S. Sutton and A. G. Barto, *Reinforcement learning: An introduction*. MIT press, 2018.
- [57] J. Schulman, F. Wolski, P. Dhariwal, A. Radford, and O. Klimov, "Proximal policy optimization algorithms," *arXiv preprint arXiv:1707.06347*, 2017.
- [58] K. Black, M. Janner, Y. Du, I. Kostrikov, and S. Levine, "Training diffusion models with reinforcement learning," *arXiv preprint arXiv:2305.13301*, 2023.
- [59] A. Mao, M. Mohri, and Y. Zhong, "Cross-entropy loss functions: Theoretical analysis and applications," in *International conference on Machine learning*. PMLR, 2023, pp. 23803–23828.
- [60] R. Zhang, K. Xiong, Y. Lu, P. Fan, D. W. K. Ng, and K. B. Letaief, "Energy efficiency maximization in ris-assisted swipt networks with rsma: A ppo-based approach," *IEEE Journal on Selected Areas in Communications*, vol. 41, no. 5, pp. 1413–1430, 2023.
- [61] N. Hand, Y. Li, Z. Slepian, and U. Seljak, "An optimal fft-based anisotropic power spectrum estimator," *Journal of Cosmology and Astroparticle Physics*, vol. 2017, no. 07, p. 002, 2017.
- [62] J. B. Kruskal, "Multidimensional scaling," *Murry Hill*, 1978.
- [63] V. C. Gungor, B. Lu, and G. P. Hancke, "Opportunities and challenges of wireless sensor networks in smart grid," *IEEE transactions on industrial electronics*, vol. 57, no. 10, pp. 3557–3564, 2010.